Fiber Bragg grating based sensing system for non-destructive root phenotyping using ResNet prediction

Steven Binder, Kabir Hossain, Alexander Bucksch, and Mable Fok

***Abstract*— Real-time measurements of crop root architecture can overcome limitations faced by plant breeders when developing climate-resilient plants. Due to current measurement methods failing to continuously monitor root growth in a non-destructive and scalable fashion, we propose a first in-soil sensing system based on fiber Bragg gratings. The sensing system continuously logs three-dimensional strain generated by a growing pseudo-root. Two ResNet models confirm the utility of in-soil fiber Bragg grating sensors and predict root width and depth from sensor output data and achieve accuracies of 92% and 93% respectively. Our presented prototype has potential prospects to go beyond measuring root parameters and sense its surrounding soil environment.**

***Index Terms*—Deep learning, Fiber Bragg grating (FBG), optical sensing, plant phenotyping, and Residual Neural Network (ResNet).**

I. INTRODUCTION

BY 2050, global population will reach upwards of 10 billion people and outpace the world's production of agricultural resources [1]. Additionally, degraded soil conditions due to climate change and overuse of land will further limit crop production. Measurement of plant root architecture in a non-destructive, continuous fashion provides a promising means of improving nutrient uptake in crops [2]. Thus, providing a mitigation strategy for the adverse effects induced by climate change. The development of a continuous root measurement system can help breeders better understand how a plant interacts with its environment so they may develop crops with improved resource uptake [3]. With breeders developing more efficient crops, farmers will then be able to maximize the amount of food produced under limited water and nutrient availability.

The development of new root measurement tools is challenged by opaque soil, while the presence of highly conductive matter puts technologies based on electromagnetic waves at their resolution limit [4]. Existing methods for plant root phenotyping include destructive excavation using the Shovelomics protocol [5, 6], X-ray tomography, magnetic resonance imaging (MRI) [7], and ground penetrating radar (GPR) [8]. While accurate, Shovelomics involves the destructive excavation of roots from soil before measurement [9], thus inferring biological meaning from only a part of the root system. GPR measures non-destructively; but its reduced throughput leads to low resolution images or inaccurate measurements [10].

X-ray, on the other hand, offers rapid measurements but limits observations to plants in growth containers of limited size due to ray absorption [11]. Therefore, restricting observations to only young plants whose phenotype has not yet been impacted by its growth container. While providing high-resolution images, MRIs require complex calibration methods and suffer from distorted measurements due to magnetic materials within the soil [12, 13].

In all cases, technicians are required to operate equipment during the measurement process, which is labor intensive and time consuming, especially for continuous time series data. Therefore, these limitations prevent the deployment of current non-destructive root phenotyping technology as autonomous sensing systems. The creation of such a system without the stated limitations would allow us to quantify a plant's growth throughout its entire life cycle.

Fiber optics sensors have advantages over traditional electronics-based sensing systems making them ideal for measuring root growth. Primarily, their immunity to signal degradation caused by ferromagnetic matter present in soil allows for deployment in a large variety of environments [14]. Other advantages include having low signal attenuation when ran over long distances, a small size that allows for close placement to a growing root without interference, and a passive construction which insures they will not interact with the growing environment [15]. Previously, fiber optic sensors have been used in above ground plant sensing, for example a wearable FBG-based sensor was created to obtain continuous measurements of a melon's shape change due to hydration losses [16]. A distributed fiber optic sensor (DFOS) was also developed for non-destructive measurement of crop root growth. The strain generated by rice roots grown in a media - washed Profile Greens Grade soil amendment was able to be captured and used in a 3D reconstruction of the root's architecture [13]. While providing promising results, underground measurements using optical sensors still prove challenging due to the various soil parameters, such as temperature, moisture content, and compactness, that change over time.

Rayleigh based distributed optical sensors require complex hardware setups and precise components to achieve accurate measurements. Additionally, they suffer from low signal-to-noise ratios due to characteristically weak power induced by Rayleigh backscatter [17]. As the strain generated by roots is generally weak, this may result in noisy measurement data. Previously, we have had promising results in measuring a deforming object within potting soil using fiber Bragg grating (FBG) sensors [18]. The FBG based setup provided optical power measurements related to the changing shape of an object

in real time.

We propose a non-destructive root phenotyping sensing system utilizing fiber Bragg grating (FBG) sensors to continuously log and transmit underground in-soil measurements to a residual neural network (ResNet) for root phenotype prediction. Our proposed sensing system utilizes reflected power measurement instead of spectral measurement from the FBGs. This is done to minimize data size and the system's overall cost. Direct correlation between sensor output and root parameters is challenging as the raw signal contains measurements of both generated strain and environmental variations, such as soil moisture content. Therefore, after logging measurements from each FBG sensor, our system utilizes two ResNet models for phenotyping root width and depth. ResNet ensures that gradient flow in the measurement data does not disappear during backpropagation learning steps [19, 20]. By including skip connections, gradients are preserved and the resulting models' capacity to capture complex relationships within data is increased.

II. Methodology

In the presented experiments, our proposed sensing system detects and differentiates pseudo-root diameter classes of 1mm or 5mm. Our models also predict pseudo-root depths ranging from 0cm to 15cm with a resolution of 1.5cm. A reflected power-based measurement allows for a highly configurable system dependent on the number of plants to be monitored. Additionally, our ResNet model transforms the sensor's complex output into root traits with known genetic underpinnings and relevance for plant breeding programs [21].

Fig. 1 illustrates the non-destructive sensing system, consisting of three FBG sensors with Bragg wavelengths of 1550.0nm, 1552.5nm, and 1553.3nm. Each FBG has its own wavelength-tunable laser diode and optical power meter for data collection. It is worth noting that the system can be simplified further by using three FBGs of the same wavelength along with one laser diode. When strain is applied to the FBGs within soil, its Bragg wavelength elongates. Due to this, each laser is tuned to a shorter wavelength resulting in a power reading 3 dB lower than the maximum possible value. By tuning to this region, the sensing setup operates in the most linear region of the FBG's reflection spectrum. The green, red, and yellow lines correspond to the 1550.0nm, 1553.3nm, and 1552.5nm FBGs, respectively. All FBGs are perpendicular to the pseudo-root during experimental trials. LabVIEW is then used to save the output data in a text file for later prediction by the ResNet models. All experiments in this study were conducted at a constant room temperature and soil moisture content. Therefore, any measurement distortion caused by these variables will be negligible. Future versions of the sensing system will include reference FBGs to further mitigate sensor crosstalk.

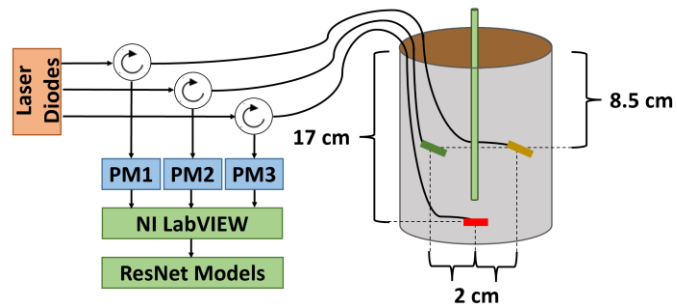

Fig. 1. The non-destructive root phenotype sensing setup.

The three sensor locations record strain generated by different regions of an aluminum pseudo-root. The two side FBGs, with wavelengths of 1550.0nm and 1552.5nm were 8.5cm below the soil surface and 2cm offset from the insertion point. By offsetting both side FBGs by 2cm, they will not physically encounter the pseudo-root. The bottom FBG, with a Bragg wavelength of 1553.3nm, was directly centered under the insertion point, 17 cm below the soil surface. Similarly to both side FBGs, an offset is used to ensure the pseudo-root and FBG did not come in contact. Each FBG was oriented such that they were perpendicular to the pseudo root for maximum strain coupling.

To efficiently generate large quantities of pseudo-growth data, we built a robotic system as shown in Fig. 2. The robot allows for the timed insertion of a pseudo-root into soil until a specific depth is reached. Controlling insertion time allows for a better correlation between sensor power change and pseudo-root parameters when training the ResNet models. Leading to higher model accuracy when tested on new data. Operated by an Arduino, the robotic system is comprised of two stepper motors that control pseudo-root movement.

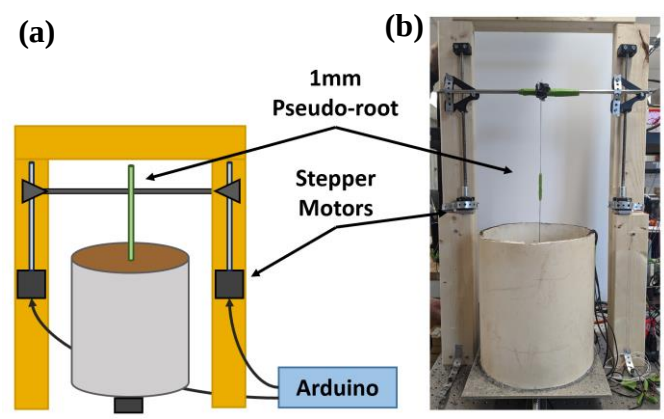

Fig. 2. (a) A schematic representation of the robotic root. (b) The physical robotic root setup.

Two pseudo-roots with diameters of 1mm and 5mm are inserted into soil to a depth of 15cm over 11 minutes to generate two datasets. 10 trials with each pseudo-root were conducted to ensure better model generalization. Raw data provided by the FBGs requires expert knowledge to be interpreted as root traits, as seen in Fig 3. Using two separate data preprocessing methods and our ResNet models, the sensor output can be transformed

into known root traits.

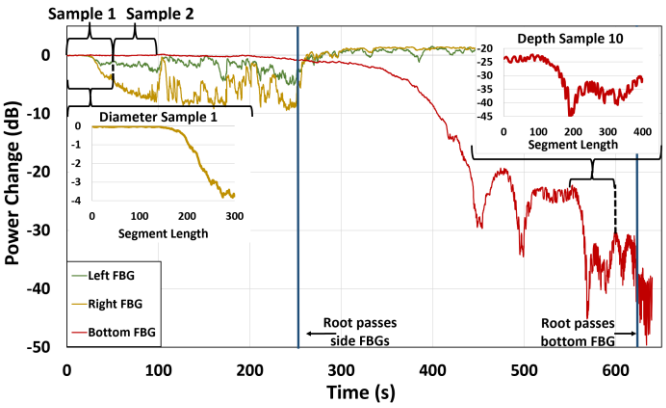

Fig. 3. The induced FBG power change by the 5mm pseudo-root and the sample processing used for each trial to generate the depth and diameter datasets

For effective ResNet model training, dataset samples must have a fixed segment length. Samples within the diameter dataset are set to have a segment length of 300 data points and are generated using both side FBGs output. Additionally, each sample contains a single root diameter. After processing, the experimental trials generated 3,228 samples. Similarly, samples within the depth dataset are generated from the bottom FBGs output and represent depth ranges between 0cm to 15cm in 1.5cm increments. Their segment lengths were set such that they contained a total of 400 data points. Preprocessing of depth data yielded a total of 300 samples for model training and validation. Fig. 3 provides an example of processed samples with fixed segment lengths. Furthermore, samples of both datasets were augmented with a sliding window approach during data segmentation. The sliding window overlapped each original segment ranging in coverage from 0% to 83.33% to help enrich the final datasets.

The diameter predicting ResNet model provides an output of one of two classes (1mm or 5mm), while the depth prediction model outputs one of the ten depth-level classes. Our proposed ResNet model's architecture, seen in Fig. 4, uses a 2x2 convolutional input layer followed by batch normalization, a Rectified Linear Unit (ReLU) activation function, and a max-pooling layer. Each max-pooling layer's output is connected to 25 residual blocks, the number of which was determined through experiments comparing computation time and model complexity. The residual blocks are then connected to two 5x5 convolution layers.

Both 5x5 convolutional layer are followed by two batch normalizations and a ReLU activation function as described in [22, 23] and contain 16 feature maps. The final residual output block from each is then connected to a global average pooling layer that feeds into three dense layers. The dense layers, valued at 50, 40, and 20, and the output layer sets the width and depth model's size to (2,1) and (10,1) for denoting diameter classes and depth levels.

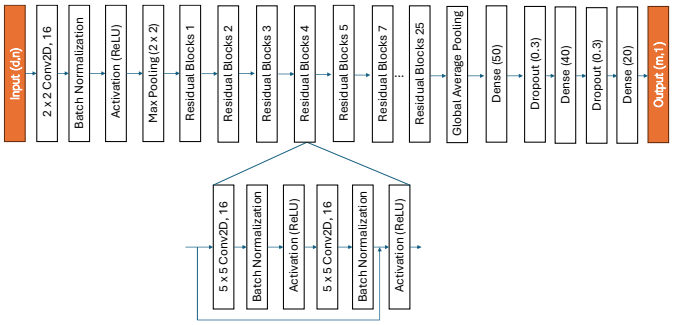

Fig. 4. Architecture of the ResNet neural networks for predicting root width and depth. n, m, and d represent the number of channels, fixed at 2, number of classes, and sample sizes, respectively.

Each dense layer is connected to a corresponding dropout layer with a rate of 0.3 to optimize network performance. When constructing machine learning models, optimizer selection is crucial for minimizing the difference between predicted and actual labels. An Adam optimizer was utilized to ensure high performance from both models. Our model implementations are available as Python code using the TensorFlow module [24] and can be found in reference [25].

III. Results and Discussion

Processed datasets were partitioned using an 80/20 split for training and testing. During the training phase, we applied dropout regularization to our ResNet model, randomly dropping units and their connections to prevent overfitting [26]. Additionally, we utilized data augmentation techniques, such as sliding window methods, to increase the size of our datasets. These protocols helped improve the model's generalization capability and mitigate the risk of overfitting.

TABLE I
PERFORMANCE METRICS OF BOTH MODELS ON THE TEST DATASETS

Model	Accuracy	Precision	TPR	FPR
Diameter	92%	90%	93%	9.20%
Depth	93%	94%	93%	0.74%

During model testing, we evaluated precision, recall, True Positive Rate (TPR), False Positive Rate (FPR), accuracy, Area Under Curve (AUC) and confusion matrices performance metrics as seen in table I. The diameter prediction model exhibits high precision and correctly predicted root diameters 90% of the time. Seen in Fig. 5(a) is an example of the diameter model's predictive results achieved from the test data. With a TPR of 93%, the model captured root diameters reliably. However, the slightly higher FPR of 9.2% suggests misclassification of negative instances as positives. We hypothesize that these misclassifications arise from the model's sensitivity towards predicting positives to achieve a higher recall. Our hypothesis is supported by the estimated recall of 93% and precision of 90%. Despite potential false alarms, this

high recall ensures that most true positives are identified. Similarities in the FBG signals provided by the different diameter classes may arise due to shared environmental factors such as soil compactness or moisture levels. These similarities could lead to the observed FPR as suggested in [27]. Nonetheless, the model's precision and recall demonstrate its effectiveness in accurate predictions among such complexities.

The depth model's precision signifies correct depth predictions 94% of the time. Additionally, its high TPR of 93% indicates the model's reliability in correctly predicting the current depth level. The low FPR of 0.74% proves the model rarely produces incorrect predictions. Fig. 5(b) shows an example of the results from our depth prediction model, where the red trace shows the predicted class provided by our ResNet model and the green trace shows the sample's actual class.

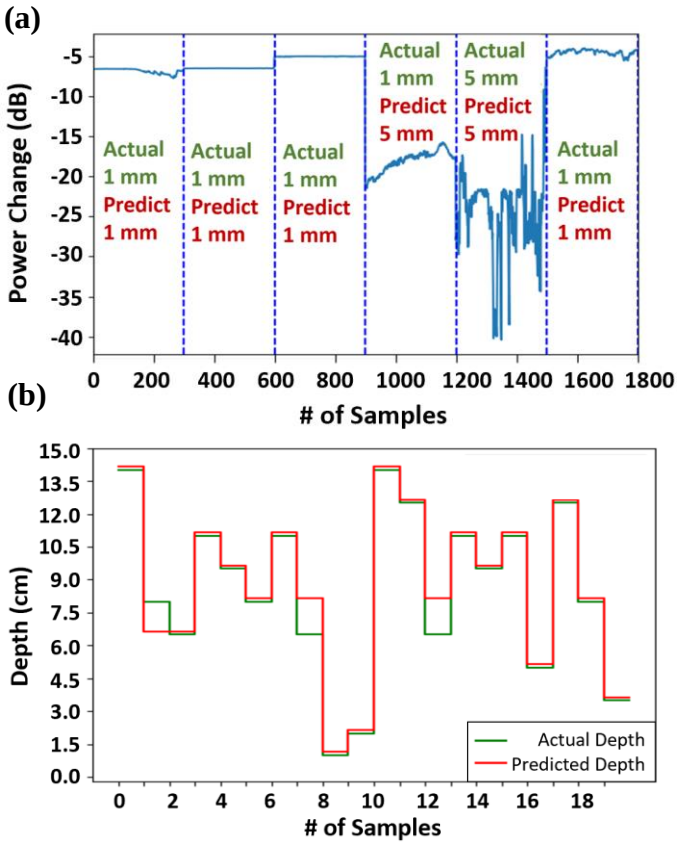

Fig. 5. Actual sample labels and predictive output of the diameter (a) and depth (b) models when tested on novel data.

Fig. 6(a) visualizes our diameter model's AUC which highlights its performance and the tradeoff that occurs between TPR and FPR. The AUC value is a quantitative measure of overall performance; a higher AUC indicates better discrimination between positive and negative instances. Seen in Fig. 6(b) is our depth model's confusion matrix produced after testing. The diagonal elements represent correct predictions for each depth level, reflecting accurate depth level identifications. Off-diagonal elements indicate instances of misclassification. For example, DL3 (Depth Level 3) contained 5 samples for model testing. Out of these, 4 were correctly identified while 1 was misclassified as indicated by the off-diagonal element.

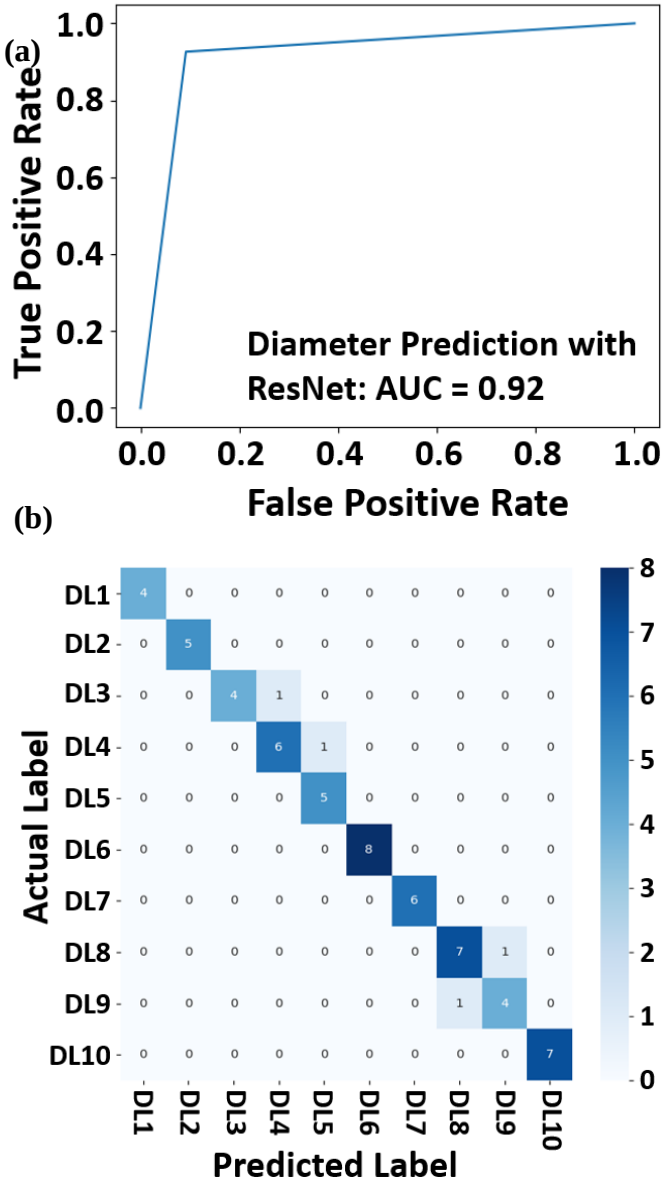

Fig. 6. (a) The diameter model's AUC curve. (b) The depth model's confusion matrix.

IV. Conclusion

In summary, we propose a non-destructive and continuous approach for quantifying root growth in real-time. Three FBGs embedded in soil paired with a ResNet deep learning model, reliably predicts a pseudo-root's diameter and depth with high accuracy. By utilizing a reflected power-based measurement setup, output data size is minimized, and additional sensors can be added easily to increase measurement resolution. Performance metrics of the two ResNet models suggest a low chance of misclassification when presented with new data. Both ResNet models convert sensor data into root trait measurements with known genetic underpinnings. Thus, our measurements will be useful to breeders for developing climate-resilient plants as we progress toward training the models on actual root growth data. While performing accurately, we do recognize the

relatively small dataset size. With base models created, our next steps include a transition to growing real crop plants under controlled environmental conditions. Using new datasets generated from actual crop plant measurements, the model's adaptability and generalization will be enhanced.

References

[1] A. Bucksch *et al.*, "Morphological Plant Modeling: Unleashing Geometric and Topological Potential within the Plant Sciences," (in English), *Front Plant Sci,* vol. 8, p. 900, Jun 9 2017, doi: 10.3389/fpls.2017.00900.

[2] J. P. Lynch, "Roots of the second green revolution," (in English), *Australian Journal of Botany,* vol. 55, no. 5, pp. 493-512, 2007, doi: 10.1071/Bt06118.

[3] J. P. Lynch, "Root phenotypes for improved nutrient capture: an underexploited opportunity for global agriculture," *New Phytol,* vol. 223, no. 2, pp. 548-564, Jul 2019, doi: 10.1111/nph.15738.

[4] W. Zheng, W. Luo, and T. Hao, "Experimental Investigations on Enhanced GPR Detection Assisted by Broadband Metasurfaces," *IEEE Transactions on Instrumentation and Measurement,* 2024.

[5] J. Burridge, C. N. Jochua, A. Bucksch, and J. P. Lynch, "Legume shovelomics: High-Throughput phenotyping of common bean (L.) and cowpea (subsp,) root architecture in the field," (in English), *Field Crops Research,* vol. 192, pp. 21-32, Jun 2016, doi: 10.1016/j.fcr.2016.04.008.

[6] J. Kengkanna, P. Jakaew, S. Amawan, N. Busener, A. Bucksch, and P. Saengwilai, "Phenotypic variation of cassava root traits and their responses to drought," (in English), *Applications in Plant Sciences,* vol. 7, no. 4, p. e01238, Apr 2019, doi: ARTN e123810.1002/aps3.1238.

[7] S. Y. Jung, S. J. Lee, and H. Park, "Investigation of water transport around the root for a plant using X-ray imaging technique," *Measurement,* vol. 151, p. 107159, 2020.

[8] W. Luo, Y. H. Lee, L. F. Ow, M. L. M. Yusof, and A. C. Yucel, "Accurate tree roots positioning and sizing over undulated ground surfaces by common offset GPR measurements," *IEEE Transactions on Instrumentation and Measurement,* vol. 71, pp. 1-11, 2022.

[9] A. Li, L. Zhu, W. Xu, L. Liu, and G. Teng, "Recent advances in methods for in situ root phenotyping," *PeerJ,* vol. 2021, p. e13638, 03/11/2021 2022, doi: 10.34133/2021/8696571.

[10] A. Srivastav, P. Nguyen, M. McConnell, K. A. Loparo, and S. Mandal, "A highly digital multiantenna ground-penetrating radar (GPR) system," *IEEE Transactions on Instrumentation and Measurement,* vol. 69, no. 10, pp. 7422-7436, 2020.

[11] P. Newill, D. Karadaglić, F. Podd, B. Grieve, and T. York, "Electrical impedance imaging of water distribution in the root zone," *Measurement Science and Technology,* vol. 25, no. 5, p. 055110, 2014.

[12] G. C. Bagnall *et al.*, "Design and demonstration of a low‐field magnetic resonance imaging rhizotron for in‐field imaging of energy sorghum roots," *The Plant Phenome Journal,* vol. 5, no. 1, p. e20038, 2022, doi: 10.1002/ppj2.20038.

[13] M. Tei, E. Barbieri, F. Soma, Y. Uga, and Y. Kawahito, "Agritech imaging of underground plant root growth using a distributed fiber optic sensor," in *Optical Fibers and Sensors for Medical Diagnostics, Treatment and Environmental Applications XXII*, San Francisco, CA, 2022 2022, vol. 11953: SPIE, pp. 98-102, doi: https://doi.org/10.1117/12.2606308.

[14] S. J. Mihailov, "Fiber Bragg grating sensors for harsh environments," *Sensors (Basel),* vol. 12, no. 2, pp. 1898-918, 2012, doi: 10.3390/s120201898.

[15] C. Pendao and I. Silva, "Optical Fiber Sensors and Sensing Networks: Overview of the Main Principles and Applications," *Sensors (Basel),* vol. 22, no. 19, p. 7554, Oct 5 2022, doi: 10.3390/s22197554.

[16] D. L. Presti *et al.*, "A wearable flower-shaped sensor based on fiber Bragg grating technology for in-vivo plant growth monitoring," *IEEE Sensors Journal,* 2023.

[17] X. Bao and Y. Wang, "Recent advancements in Rayleigh scattering-based distributed fiber sensors," *Advanced devices & instrumentation,* 2021.

[18] S. Binder, K. Hossain, B. Alexander, and F. Mable, "Non-Destructive Underground Fiber Bragg Grating Sensing System with ResNet Prediction for Root Phenotyping," presented at the SPIE Photonics Europe, Strasbourg, France, 2024.

[19] Y. Bengio, P. Simard, and P. Frasconi, "Learning Long-Term Dependencies with Gradient Descent Is Difficult," (in English), *Ieee Transactions on Neural Networks,* vol. 5, no. 2, pp. 157-166, Mar 1994, doi: Doi 10.1109/72.279181.

[20] X. Glorot and Y. Bengio, "Understanding the difficulty of training deep feedforward neural networks," in *Proceedings of the thirteenth international conference on artificial intelligence and statistics*, 2010: JMLR Workshop and Conference Proceedings, pp. 249-256.

[21] W. Ren *et al.*, "Genome-wide dissection of changes in maize root system architecture during modern breeding," *Nat Plants,* vol. 8, no. 12, pp. 1408-1422, Dec 2022, doi: 10.1038/s41477-022-01274-z.

[22] K. He, X. Zhang, S. Ren, and J. Sun, "Deep residual learning for image recognition," in *Proceedings of the IEEE conference on computer vision and pattern recognition*, 2016, pp. 770-778.

[23] J. Li, P. Fearnhead, P. Fryzlewicz, and T. Wang, "Automatic change-point detection in time series via deep learning," *arXiv preprint arXiv:2211.03860,* 2022.

[24] V. Ivan, *Python deep learning: exploring deep learning techniques and neural network architectures with PyTorch, Keras, and TensorFlow*. Packt Publishing, 2019.

[25] K. Hossain. "Root-Diameter-Prediction-with-Residual-Neural-Network." https://wave.engr.uga.edu/code/ (accessed.

[26] N. Srivastava, G. Hinton, A. Krizhevsky, I. Sutskever, and R. Salakhutdinov, "Dropout: a simple way to prevent neural networks from overfitting," *The journal of machine learning research,* vol. 15, no. 1, pp. 1929-1958, 2014.

[27] A. Kharkar *et al.*, "Learning to reduce false positives in analytic bug detectors," in *Proceedings of the 44th International Conference on Software Engineering*, 2022, pp. 1307-1316.